

Theoretical Exploration of Phase Transitions in a Cavity-BEC System with Two Crossed Optical Pumps

Wei Qin,^{*} Dong-Chen Zheng,^{*} Zhao-Di Wu, Yuan-Hong Chen, and Renyuan Liao[†]
*Fujian Provincial Key Laboratory for Quantum Manipulation and New Energy Materials,
College of Physics and Energy, Fujian Normal University, Fuzhou 350117, China and
Fujian Provincial Collaborative Innovation Center for Advanced High-Field
Superconducting Materials and Engineering, Fuzhou, 350117, China*

(Dated: March 4, 2025)

We consider a Bose-Einstein condensation (BEC) inside an optical cavity and two crossed coherent pump fields. We determine the phase boundary separating the normal superfluid phase and the superradiance phase, perturbatively. In the regime of negative cavity detuning, we map out the phase diagrams both for an attractive and a repulsive optical lattice. It turns out that the situation is quite different in two cases. Specifically, in the case of attractive lattice, if a system is in the superradiant phase with one pump laser, adding another pump does not drive the system out of the superradiance phase. While for the repulsive lattice, increasing another pump potential have suppressive effects on the superradiance. We also find that, in the case of attractive lattice, equally increasing two pump lattice potentials can induce a transition from the normal phase to the superradiance phase. In stark contrast, for the repulsive lattice, the system will remain in the normal phase as the pump depths are tuned within a wide range, independent of the cavity detuning and the decay rate.

I. INTRODUCTION

Loading ultracold quantum gases into single or multiple high-finesse cavities provides a versatile platform to explore many-body phenomena [1–11]. The coupling between the degenerate quantum gases and quantized radiation fields in cavities gives rise to controllable long-range interactions, which is dominant in many-body phases [12, 13]. Transversely driving a Bose-Einstein condensation (BEC) inside an optical cavity is such a typical example, and it allows to achieve the Dicke model and a self-organization phase [12, 14–21]. Taking the atoms' spins into account, one single cavity can also mediate spin-dependent interactions, realize single-mode Dicke spin-models [22–25], and simulate a nondegenerate two-mode Dicke model [26, 27]. With two crossed linear cavities, it is possible to demonstrate the coupling between two order parameters [28–30], realize different supersolid formation, and even engineer a continuous $U(1)$ symmetry in real space and cavity space [31–34], so that Higgs and Goldstone modes can be monitored and manipulated [35].

Scattering photons into cavities, accompanied with the self-organization of quantum gases, lies at the heart of these phenomena, which is also referred as the superradiance. Usually, an attractive potential, rather than a repulsive one, is expected to induce the superradiance. Since, intuitively, the buildup of any additional repulsive potential seems to cost energy, and hence prohibits self-organization. Actually, most of experiments implement a red-detuned pump laser to drive atoms, so that an

attractive standing wave lattice can be generated. However, a repulsive pump potential, generated by a blue-detuned optical pump, is also able to produce the superradiance, which has been verified theoretically and experimentally [36–40].

In practice, such a cavity-BEC system is commonly driven by a single pump laser. It is hard to resist the temptation to ask: what if there are more than just one pump? And what is the situation in the case of an attractive or a repulsive optical lattice? It is not a trivial question to answer since additional pumps produce a two-dimensional periodic potential and lower the symmetry of the system, as compared with the case of one pump. In this work, we address this question by considering a cavity-BEC system in the presence of two crossed optical pumps, and we also take the interference between the two pumps into account. By mapping out the phase diagrams, we conclude that adding another pump will increase the tendency of transition towards the superradiance in the case of attractive lattice, and suppress the tendency in the case of repulsive lattice. We also find that the repulsive rectangular lattice (equal pump lattice depths) can not induce the superradiance within a wide range of pump depths, which is independent of cavity detuning and decay rate.

II. MODEL AND FORMALISM

We consider a BEC (orange) inside a high-finesse optical Fabry-Pérot resonator is exposed to a cavity laser beam (yellow) and two pump laser beams (green and blue). The angle between the cavity beam and per pump beam is 60° , as shown in FIG. 1(a). We focus on the two-dimensional case, where the atoms' motion along \hat{z} can be frozen by tight confinement and bosons can only move

^{*} These authors contributed equally to this work.

[†] rylliao@fjnu.edu.cn

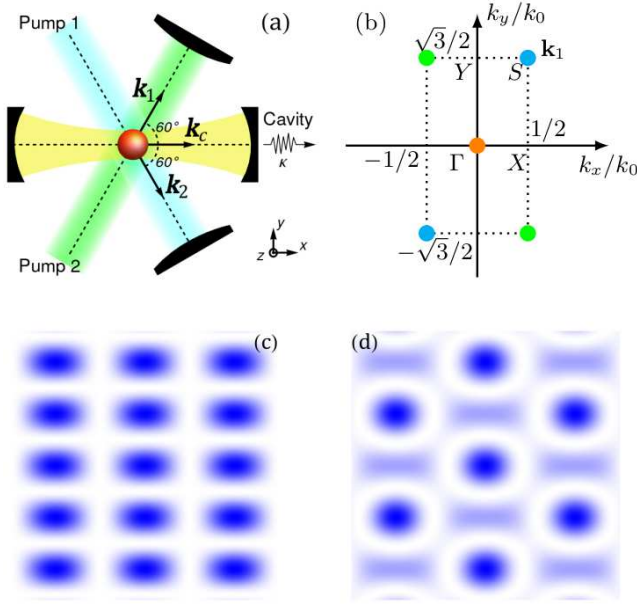


FIG. 1. (a) Schematic of the experimental setup. A BEC (orange) inside a high-finesse optical resonator is exposed to pump laser beam 1 (green) and pump laser beam 2 (blue). Photons scattered by the atoms populate the cavity mode (yellow), with coherent field amplitude α that can be detected when leaking from the cavity. The angles between the cavity beam and per pump beam are both 60° . (b) Wave vector (momentum) distributions of the BEC. Orange point marks the condensed state in absence of photons scattering into the cavity, while green (blue) point is steady state of condensation scattered by pump 1 (2) in superradiant phase. The dotted line is the boundary of the first Brillouin zone for the two dimensional rectangular lattice of the combined pump fields. (c) and (d) are calculated density modulations for equal pump lattice depths without and with the intracavity field, respectively, for red atomic detuning $\Delta_a < 0$. In the case of $\Delta_a > 0$, there is no superradiant phase under equal pump depths within red atomic detuning $\Delta_c < 0$, but still has the same density pattern as (c) in absence of intracavity field.

in the xy plane [41]. The decay rate of the cavity field is κ . Within dipole and rotating-wave approximation, the effective many-body Hamiltonian in a frame rotating at the pump laser frequency [1, 27] is given by

$$\hat{H} = \int d\mathbf{r} \hat{\Psi}^\dagger(\mathbf{r}) \left(\frac{\hat{\mathbf{p}}^2}{2m} + \frac{\hbar}{\Delta_a} \hat{\mathbf{E}}^\dagger \hat{\mathbf{E}} \right) \hat{\Psi}(\mathbf{r}) - \hbar \Delta_c \hat{a}^\dagger \hat{a}, \quad (1a)$$

$$\hat{\mathbf{E}} = \sum_{i=1,2} \Omega_i \cos(\mathbf{k}_i \cdot \mathbf{r}) + g \cos(\mathbf{k}_c \cdot \mathbf{r}) \hat{a}, \quad (1b)$$

where $\hat{\Psi}^\dagger(\hat{\Psi})$ is the creation (annihilation) operator for bosonic atoms with mass m and momentum $\hat{\mathbf{p}} = -i\hbar\nabla$. $\hat{a}^\dagger(\hat{a})$ is the photon creation (annihilation) operator for the cavity mode. Here we consider pump beams have the same frequency ω_p , which is far detuned by $\Delta_a = \omega_p - \omega_a$ from the atomic resonance at frequency ω_a . The cavity frequency ω_c is closely detuned by $\Delta_c = \omega_p - \omega_c$ from

the pump frequency, and we only stay within $\Delta_c < 0$ throughout this work. Ω_j with $j = 1, 2$ are the Rabi frequencies for pump beams, g is single-photon Rabi frequency of the cavity mode. The wave vectors of the pump beams and cavity light are given by $\mathbf{k}_j = k_0 \cos(60^\circ)\hat{x} + (-1)^{j+1}k_0 \sin(60^\circ)\hat{y}$ and $\mathbf{k}_c = k_0\hat{x}$ respectively, as denoted in FIG. 1(a). Here k_0 is the wave-vector magnitude of the pumping lasers and the cavity mode. We choose recoil energy $E_R = \hbar^2 k_0^2 / 2m$ as energy unit, and set $\hbar = 1$ for simplicity.

At zero temperature limit, all atoms occupy the lowest-energy Bloch state $|\Psi^{(1)}(0)\rangle$ in absence of intracavity photons, where $|\Psi^{(j)}(\mathbf{k})\rangle$ denotes the j -th band eigenstates of the single-particle Hamiltonian

$$\hat{\mathcal{H}}_0 = \frac{\hat{\mathbf{p}}^2}{2m} + \text{sgn}(\Delta_a) \left[V_1 \cos^2(\mathbf{k}_1 \cdot \mathbf{r}) + V_2 \cos^2(\mathbf{k}_2 \cdot \mathbf{r}) + 2\sqrt{V_1 V_2} \cos(\mathbf{k}_1 \cdot \mathbf{r}) \cos(\mathbf{k}_2 \cdot \mathbf{r}) \right]. \quad (2)$$

Here we defined pump lattice depths $V_i = \Omega_i^2 / |\Delta_a|$ with $i = 1, 2$, and $\text{sgn}(\Delta_a)$ gives the sign of atomic detuning Δ_a . Indeed, $\text{sgn}(\Delta_a)$ determines whether the effective pump potential is attractive (negative) or repulsive (positive).

In the presence of intracavity photons, they are scattered by atoms from the transverse pump lasers into the cavity mode and vice versa. It is sufficient to consider the two-photon scattering processes through the phase transition. Equivalently, starting from the lowest-energy Bloch state $|\Psi^{(1)}(0)\rangle$ of BEC, only $|\Psi^{(j)}(\mathbf{k}_1)\rangle$ can be reached by applying scattering operator

$$\hat{\Theta} = \sum_{i=1,2} \sqrt{V_i} \cos(\mathbf{k}_i \cdot \mathbf{r}) \cos(\mathbf{k}_c \cdot \mathbf{r}). \quad (3)$$

Hence the atomic field operator can be expanded as

$$\hat{\Psi}(\mathbf{r}) \approx \langle \mathbf{r} | \Psi^{(1)}(0) \rangle \hat{b}_0 + \sum_j \langle \mathbf{r} | \Psi^{(j)}(\mathbf{k}_1) \rangle \hat{b}_j, \quad (4)$$

where \hat{b}_0 and \hat{b}_j are bosonic annihilation operators for states $|\Psi^{(1)}(0)\rangle$ and $|\Psi^{(j)}(\mathbf{k}_1)\rangle$ respectively. The sums are over all band index $j = 1, 2, \dots$, whilst the particle number conservation $\hat{b}_0^\dagger \hat{b}_0 + \sum_j \hat{b}_j^\dagger \hat{b}_j = N$ should be satisfied, with N being the total atom number. Substituting Eq. (4) into Eq. (1) yields the effective Hamiltonian

$$\begin{aligned} \hat{H}_{\text{eff}} = & -\tilde{\Delta}_c \hat{a}^\dagger \hat{a} + \sum_j (E_j - E_0) \hat{b}_j^\dagger \hat{b}_j \\ & + (\hat{a}^\dagger + \hat{a}) \sum_j \left(\nu_j \hat{b}_j^\dagger \hat{b}_0 + h.c. \right), \end{aligned} \quad (5)$$

where the effective cavity detuning is defined as $\tilde{\Delta}_c = \Delta_c - \text{sgn}(\Delta_a) U_0 N \langle \Psi^{(1)}(0) | \cos^2(\mathbf{k}_c \cdot \mathbf{r}) | \Psi^{(1)}(0) \rangle$, and here we set $U_0 = g^2 / |\Delta_a|$. The scattering matrix elements are given by $\nu_j = \text{sgn}(\Delta_a) \sqrt{U_0} \theta_j$ with $\theta_j =$

$\langle \Psi^{(j)}(\mathbf{k}_1) | \hat{\Theta} | \Psi^{(1)}(0) \rangle$. E_0 and E_j are eigenvalues of $\hat{\mathcal{H}}_0$ corresponding to $|\Psi^{(1)}(0)\rangle$ and $|\Psi^{(j)}(\mathbf{k}_1)\rangle$, respectively.

We proceed with mean-field description by taking the average values $\langle \hat{a} \rangle = \alpha$, $\langle \hat{b}_0 \rangle = \psi_0$, and $\langle \hat{b}_j \rangle = \psi_j$. The atomic fields are governed by Heisenberg equations $i\partial_t \hat{b}_j = [\hat{b}_j, \hat{H}_{\text{eff}}]$. We seek a steady state in which $\partial_t \psi_j = 0$, gaining $\psi_j = (\alpha^* + \alpha) \nu_j \psi_0 / (E_0 - E_j)$. Together with the normalization condition $|\psi_0|^2 = N - \sum_j |\psi_j|^2$, we retain the ground state energy up to the fourth order in amplitude of α ,

$$\mathcal{E}_\alpha \approx -\tilde{\Delta}_c \alpha^* \alpha - NU_0 \chi (\alpha^* + \alpha)^2 + NU_0^2 \chi \eta (\alpha^* + \alpha)^4, \quad (6)$$

here we have defined the susceptibility $\chi = \sum_j |\theta_j|^2 / (E_j - E_0)$, and $\eta = \sum_j |\theta_j|^2 / (E_j - E_0)^2$. Note that χ and η are function of V_1, V_2 , and they also depend on $\text{sgn}(\Delta_a)$. Meanwhile, the Heisenberg equation of photon operator is given by $i\partial_t \hat{a} = [\hat{a}, \hat{H}_{\text{eff}}] - i\kappa \hat{a}$. The steady condition $\partial_t \alpha = 0$ leads to $\alpha = \text{sgn}(\Delta_a) \sqrt{U_0} \Theta / (\tilde{\Delta}_c + i\kappa)$, where an order parameter $\Theta = \int d\mathbf{r} \langle \hat{\Psi}^\dagger \hat{\Theta} \hat{\Psi} \rangle$ has been introduced, so that energy can be transformed into

$$\mathcal{E}_\Theta \approx -\frac{\tilde{\Delta}_c U_0}{\tilde{\Delta}_c^2 + \kappa^2} \left(1 + \frac{4\tilde{\Delta}_c NU_0 \chi}{\tilde{\Delta}_c^2 + \kappa^2} \right) \Theta^2 + \frac{16\tilde{\Delta}_c^4 NU_0^4 \chi \eta}{(\tilde{\Delta}_c^2 + \kappa^2)^4} \Theta^4. \quad (7)$$

The coefficient of the forth-order term being positive guarantees the stability of system. We minimize the ground state energy Eq. (7) with respect to the order parameter Θ , yielding the established superradiant phase condition

$$-\frac{4\tilde{\Delta}_c NU_0}{\tilde{\Delta}_c^2 + \kappa^2} \chi > 1. \quad (8)$$

Note that we only deal with $\tilde{\Delta}_c < 0$ here. In the normal phase, we have $\Theta = 0$ as expected; while in the superradiance, system has to choose among the two solutions

$$\Theta = \pm \frac{N\eta\chi(\tilde{\Delta}_c^2 + \kappa^2)\sqrt{\tilde{\Delta}_c^2 + \kappa^2 + 4NU_0\tilde{\Delta}_c\chi}}{4\sqrt{2}(NU_0\tilde{\Delta}_c\eta\chi)^{3/2}}. \quad (9)$$

In fact, the effective Hamiltonian Eq. (5) possesses a \mathbb{Z}_2 symmetry, as it is invariant under simultaneous transformation $\hat{a} \rightarrow -\hat{a}$ and $\hat{b}_j \rightarrow -\hat{b}_j$. The system spontaneously breaks this \mathbb{Z}_2 symmetry during the transition from the normal superfluid to the superradiance [42].

III. RESULTS AND DISCUSSION

The key part of phase condition Eq. (8) is the susceptibility χ of the normal phase, which characterizes the tendency of inducing superradiance. A larger χ indicates a greater critical magnitude of effective cavity

detuning $|\tilde{\Delta}_c|$. Since we have taken the interference between two pumping lasers into account, the relations of χ to V_1 and V_2 can not be separated independently, i.e., $\chi(V_1, V_2) \neq \chi_1(V_1)\chi_2(V_2)$, so it is infeasible to directly apply outcomes derived from single-pump case for simplicity.

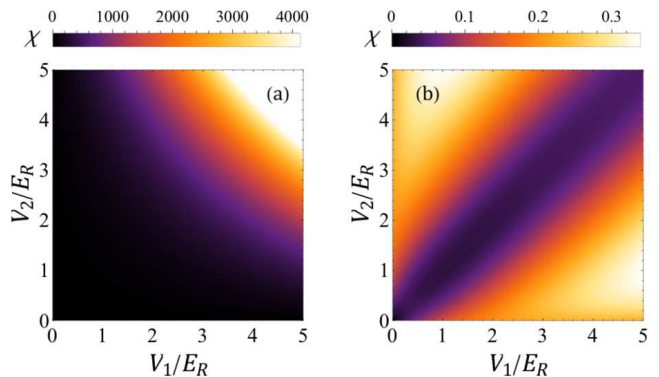


FIG. 2. Susceptibility χ as a function of V_1 and V_2 for (a) $\Delta_a < 0$ and (b) $\Delta_a > 0$. The brightness of the region is proportional to the magnitude of χ . A brighter region represents a larger χ .

We present numerical results for χ at zero temperature in FIG. 2 for different sign of atomic detuning Δ_a . In both cases, the susceptibility shows non-negativity $\chi \geq 0$. As expected, it is symmetric about $V_1 = V_2$, which renders that it is equivalent to fix one of the pump depths while varying another. However, in the case of $\Delta_a < 0$, χ grows as V_1 increases at given V_2 ; while for $\Delta_a > 0$, this monotonicity disappears as V_2 rises, and χ decreases to a local minimum towards $V_1 = V_2$. Furthermore, the growth rate of χ connected with $\Delta_a < 0$ is much larger than that with $\Delta_a > 0$. Within the range of $V_1, V_2 \in [0, 5E_R]$, the maximum χ_{max} is over 4000 in FIG. 2(a), in comparison to $\chi_{\text{max}} \sim 0.34$ in FIG. 2(a). This can be understood from the fact that the pump depths flatten the energy bands, as indicated in FIG. 3. Here, we only plot two lowest bands, which contribute the major parts of χ . Without loss of generality, pump depths are set to be equal, so that pump potentials form rectangular lattice, as shown in FIG. 1(a). It is clear that increasing pump depths has a much more powerful effect on flattening energy bands and widening band gaps with negativity than positivity of Δ_a . Especially the first band width $E_1 - E_0$, which determines the denominator of the leading term in χ , becomes dominant at higher pump depths.

With susceptibility χ in hand, we are now in a position to construct phase diagrams. The pump lattice depths V_1, V_2 can be tuned by varying the pump laser power, while cavity detuning Δ_c can be controlled via cavity frequency ω_c . For experimental consideration, we shall construct phase diagrams in terms of experimentally tunable parameters V_1, V_2 and Δ_c .

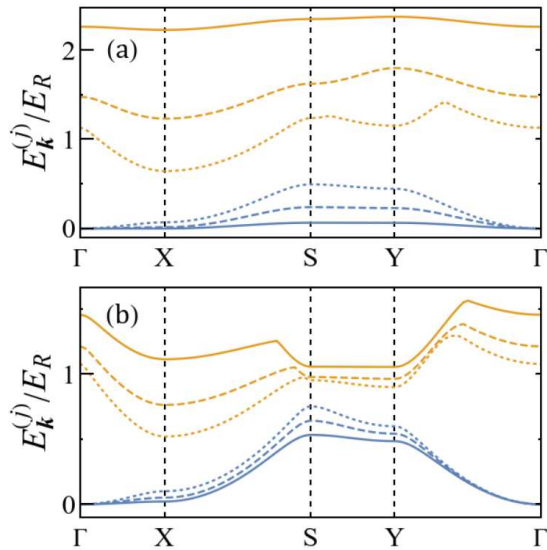


FIG. 3. Lowest two bands of rectangular pump lattice for equal pump depths, $V_1 = V_2$, with (a) $\Delta_a < 0$ and (b) $\Delta_a > 0$. Dotted, dashed and solid lines are numerical results of pump lattice depths $0.5E_R$, E_R and $2E_R$, respectively. Bands are calculated along points Γ , X , S and Y marked in FIG. 1(a).

A. Phase Diagrams Spanned by V_1 and Δ_c

Solving phase boundary condition of Eq. (8) with respect to Δ_c , yields the critical cavity detuning

$$\frac{\Delta_{\pm}}{NU_0} = \text{sgn}(\Delta_a)\theta_c - 2\chi \pm \sqrt{4\chi^2 - \left(\frac{\kappa}{NU_0}\right)^2}, \quad (10)$$

where we additionally define scattering matrix element $\theta_c = \langle \Psi^{(1)}(0) | \cos^2(\mathbf{k}_c \cdot \mathbf{r}) | \Psi^{(1)}(0) \rangle$ for convenience. It turns out that θ_c can not be neglected when $\Delta_a > 0$, as θ_c is comparable with χ .

Here, we only consider the situation that $\Delta_c < 0$. The reason is that: for $\Delta_c > 0$, the term $-\Delta_c \hat{a}^\dagger \hat{a}$ in Eq. (1) indicates that the system can lower its energy in the rotating frame with more photons, and then gives rise to a transition from metastable regime to unstable regime [40]. In this situation, we have to care about large α , and therefore, perturbation method breaks down. Instead, within $\Delta_c < 0$, we only need to deal with small α , and the above results always hold. Hence, only negative solutions of Eq. (10) have been taken into account. We map out phase diagrams on V_1 and Δ_c at small V_2 in FIG. 4. Here, we choose the parameters from Ref. [40] for verification, where atoms number $N = 2.7 \times 10^5$, decay rate $\kappa = 2\pi \times 147$ kHz, atom-cavity coupling $g = 2\pi \times 1.95$ MHz and magnitude of atomic detuning $|\Delta_a| = 2\pi \times 76.6$ GHz.

For $\Delta_a < 0$, Δ_{\pm} are both negative due to $\chi > 0$ and $\theta_c > 0$. At the limit $V_2 \rightarrow 0$, phase boundary in FIG. 4(a) captures the characteristics of the well-known superradiant transition in single-pump system: the cavity photons emerge and then vanish as the cavity detuning in-

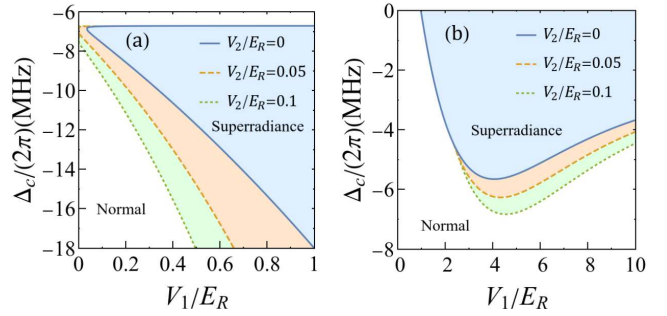


FIG. 4. Phase diagrams spanned by one of pump lattice depths V_1 and cavity detuning Δ_c for (a) $\Delta_a < 0$ and (b) $\Delta_a > 0$. Another pump depth is fixed at small value, $V_2/E_R < 1$. Experimental settings in Ref. [40] are used, where atoms number $N = 2.7 \times 10^5$, decay rate $\kappa = 2\pi \times 147$ kHz, atom-cavity coupling $g = 2\pi \times 1.95$ MHz and magnitude of atomic detuning $|\Delta_a| = 2\pi \times 76.6$ GHz.

creasing from below [12]. And there is a threshold of V_1 , here $V_1 \sim 0.03E_R$, below which the superradiance will not happen. The threshold can be obtained by requiring $\chi = \kappa/(2NU_0)$. However, this threshold will no longer exist while another pump depth V_2 rises, as exhibited by the boundaries of $0.05E_R$ and $0.1E_R$ in FIG. 4(a). In other words, if a system is in the superradiant phase with one pump laser, adding another pump will not drive it out. And increasing V_2 also makes the lower bounds of phase boundaries steeper and steeper, and indicates the system is easier to enter superradiant phase.

However, situations are different in the case of $\Delta_a > 0$, where $\theta_c \sim 0.5$ is comparable with χ . And that leaves only Δ_- being partially negative as a function of V_1 at current parameter settings. At the limit $V_2 \rightarrow 0$, phase boundary in FIG. 4(b) is in agreement with the numerical mean-field results in Ref. [40]. For a fixed cavity detuning Δ_c , such as $-2\pi \times 4$ MHz, the system starting in the normal phase undergoes a transition to the superradiant phase and comes back to the normal phase as pump lattice is ramped up. This uniqueness of the phase boundary is a result of the competition between band gap and mode softening. Meanwhile, there is a local minimum of critical Δ_c for different V_2 , and it gets lower as V_2 increases.

In the regime of a deeper pump lattice, $V_2/E_R > 1$, the slope of critical cavity detuning Δ_- , as a function of V_1 , gets even more steeper than in $V_2/E_R < 1$ for negative Δ_a , as shown in FIG. 5(a). It indicates the increasing tendency of transition towards superradiance as the pump depth goes deeper, provided that the pump lattice potentials are both attractive.

While for positive Δ_a , another superradiant region shows up at higher pump depths, $V_2/E_R > 1$. In this regime, the system enters the superradiant phase, comes back to the normal phase, and then reenters into the superradiance as pump depth V_1 is ramped up, as illustrated in FIG. 5(a). In contrast to the case in $\Delta_a < 0$, if a system is in the superradiant phase with single pump

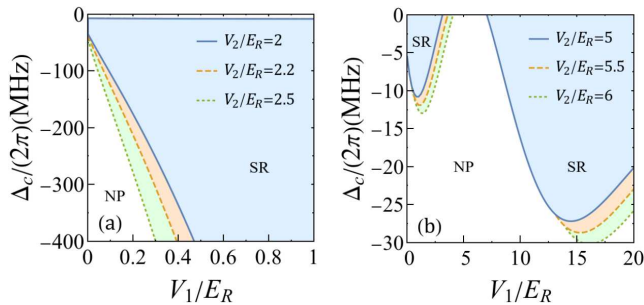


FIG. 5. Phase diagrams spanned by one of pump lattice depths V_1 and cavity detuning Δ_c for (a) $\Delta_a < 0$ and (b) $\Delta_a > 0$. Another pump depth is fixed at comparable value, $V_2/E_R > 1$. Other parameters are set to be the same as FIG. 4. The acronym NP stands for the Normal Phase, and SR for Superradiance.

laser, adding another pump will suppress superradiance within a certain range.

B. Phase Diagrams Spanned by V_1 and V_2

In phase boundary condition of Eq. (8), not only χ , but also θ_c in $\tilde{\Delta}_c$ has the dependence on V_1 and V_2 . It is useful to introduce functions f_{\pm} for $\text{sgn}(\Delta_a) = \pm 1$, where

$$f_{\pm} = \chi + \frac{[\Delta_c/(NU_0) \mp \theta_c]^2 + [\kappa/(NU_0)]^2}{4[\Delta_c/(NU_0) \mp \theta_c]}. \quad (11)$$

Note that f_{\pm} are dimensionless functions of V_1/E_R and V_2/E_R if $\Delta_c/(NU_0)$ and $\kappa/(NU_0)$ are given. $\tilde{\Delta}_c < 0$ and $\Delta_c < 0$ restrict $\Delta_c/(NU_0) < 0$ for $\Delta_a > 0$ and $\Delta_c/(NU_0) < -\theta_c$ for $\Delta_a < 0$. Here, $f_{\pm} > 0$ are the criteria for superradiance, and $f_{\pm} < 0$ for the normal phase. In FIG. 6, we plot the phase diagrams for different cavity detunings $\Delta_c/(NU_0)$ at decay rate $\kappa/(NU_0) = 0.1$.

Within $V_1, V_2 \leq 5E_R$, the area of the normal phase shrinks as Δ_c approaches 0 for both positive and negative Δ_a , in accordance with the above results. Now, if we keep two pump depths equal, $V_1 = V_2$, and increase them simultaneously, the system undergoes a transition from the normal phase to superradiance in the case of positive Δ_a ; while for negative Δ_a , the system remains in the normal phase. Notice that there exists a diagonal region around $V_1 = V_2$ for the normal phase when $\Delta_a > 0$, even if Δ_c approaches zero, as shown in FIG. 6(a). Actually, one can derive that $f_+ < \chi - \theta_c/4$ is true for arbitrary $V_1, V_2 > 0$ in this case. Numerical results show that $\chi - \theta_c/4 \sim -0.1$, thereby $f_+ < 0$, as two equal pump depths $V_1 = V_2 = V$ change within $10E_R$. In other words, if two pump depths are equal, the system will remain in the normal phase as pump depths increases

within a wide range (at least from 0 to $10E_R$), no matter how we choose κ and Δ_c . The same arguments apply to the neighborhoods of $V_1 = V_2$. From another point of view, if a system is in the superradiant phase with single pump of depth V_1 , adding another pump of V_2 will suppress superradiance for $V_2 \leq V_1$.

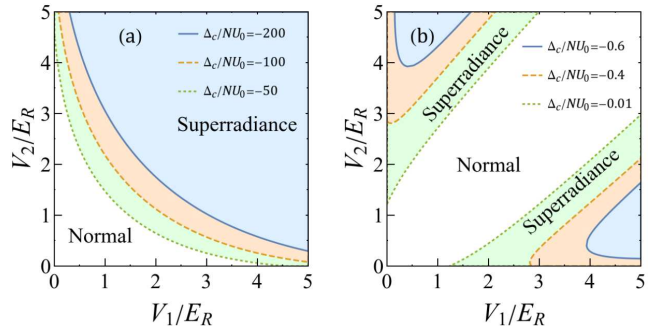


FIG. 6. Phase diagrams in terms of two pump lattice depths V_1 and V_2 with cavity detuning Δ_c fixed for (a) $\Delta_a < 0$ and (b) $\Delta_a > 0$. Here we set $\kappa/(NU_0) = 0.1$.

IV. CONCLUSION

We compare susceptibilities of a BEC inside two crossed pump fields for the red atomic detuning ($\Delta_a < 0$) and the blue atomic detuning ($\Delta_a > 0$). We map out phase boundaries separating the normal superfluid and the superradiance for the red cavity detuning ($\Delta_c < 0$). Phase diagrams are examined at the single pump limit, and they are also compared in the double pump regime. We find that if a system is in the superradiant phase with one pump laser, adding another pump will remain in the superradiance when the atomic detuning is red ($\Delta_a < 0$). While for the blue detuning ($\Delta_a > 0$), increasing another pump potential have a suppressive effect on the superradiance. Finally, we show that equally increasing two pump potentials can also induce a transition from the normal phase to superradiance for red atomic detuning ($\Delta_a < 0$). While in the case of blue detuning ($\Delta_a > 0$), the system will remain in the normal phase as pump depths increasing within a wide range, and it is independent of cavity detuning and decay rate. Experimental verifications of our predictions are believed to contribute to a better understanding of superradiance transitions with ultracold gases in optical cavities.

ACKNOWLEDGMENTS

This work is supported by NSFC under Grants No.12174055 and No.11674058, and by the Natural Science Foundation of Fujian under Grant No. 2020J01195.

-
- [1] H. Ritsch, P. Domokos, F. Brennecke, and T. Esslinger, Cold atoms in cavity-generated dynamical optical potentials, *Rev. Mod. Phys.* **85**, 553 (2013).
- [2] V. D. Vaidya, Y. Guo, R. M. Kroeze, K. E. Ballantine, A. J. Kollár, J. Keeling, and B. L. Lev, Tunable-range, photon-mediated atomic interactions in multimode cavity qed, *Phys. Rev. X* **8**, 011002 (2018).
- [3] F. Mivehvar, F. Piazza, T. Donner, and H. Ritsch, Cavity QED with quantum gases: new paradigms in many-body physics, *Advances in Physics* **70**, 1 (2021).
- [4] S. Ostermann, H. Ritsch, and F. Mivehvar, Many-body phases of a planar Bose-Einstein condensate with cavity-induced spin-orbit coupling, *Phys. Rev. A* **103**, 023302 (2021).
- [5] P. Kongkhambut, J. Skulte, L. Mathey, J. G. Cosme, A. Hemmerich, and H. Keßler, Observation of a continuous time crystal, *Science* **377**, 670 (2022).
- [6] D. Dreon, A. Baumgärtner, X. Li, S. Hertlein, T. Esslinger, and T. Donner, Self-oscillating pump in a topological dissipative atom-cavity system, *Nature* **608**, 494 (2022).
- [7] S. Ostermann, V. Walther, and S. F. Yelin, Superglass formation in an atomic BEC with competing long-range interactions, *Phys. Rev. Res.* **4**, 023074 (2022).
- [8] L. Carl, R. Rosa-Medina, S. D. Huber, T. Esslinger, N. Dogra, and T. Dubcek, Phases, instabilities and excitations in a two-component lattice model with photon-mediated interactions, *Phys. Rev. Res.* **5**, L032003 (2023).
- [9] J. Skulte, P. Kongkhambut, S. Rao, L. Mathey, H. Keßler, A. Hemmerich, and J. G. Cosme, Condensate Formation in a Dark State of a Driven Atom-Cavity System, *Phys. Rev. Lett.* **130**, 163603 (2023).
- [10] Y. Deng and S. Yi, Self-ordered supersolid phase beyond Dicke superradiance in a ring cavity, *Phys. Rev. Res.* **5**, 013002 (2023).
- [11] N. Sauerwein, F. Orsi, P. Urich, S. Bandyopadhyay, F. Mattiotti, T. Cantat-Moltrecht, G. Pupillo, P. Hauke, and J.-P. Brantut, Engineering random spin models with atoms in a high-finesse cavity, *Nat. Phys.* **19**, 1128 (2023).
- [12] K. Baumann, C. Guerlin, F. Brennecke, and T. Esslinger, Dicke quantum phase transition with a superfluid gas in an optical cavity, *Nature* **464**, 1301 (2010).
- [13] N. Defenu, T. Donner, T. Macrì, G. Pagano, S. Ruffo, and A. Trombettoni, Long-range interacting quantum systems, *Rev. Mod. Phys.* **95**, 035002 (2023).
- [14] R. H. Dicke, Coherence in Spontaneous Radiation Processes, *Phys. Rev.* **93**, 99 (1954).
- [15] C. Maschler, I. B. Mekhov, and H. Ritsch, Ultracold atoms in optical lattices generated by quantized light fields, *The European Physical Journal D* **46**, 545 (2008).
- [16] D. Nagy, G. Szirmai, and P. Domokos, Self-organization of a Bose-Einstein condensate in an optical cavity, *The European Physical Journal D* **48**, 127 (2008).
- [17] D. Nagy, G. Kónya, G. Szirmai, and P. Domokos, Dicke-Model Phase Transition in the Quantum Motion of a Bose-Einstein Condensate in an Optical Cavity, *Phys. Rev. Lett.* **104**, 130401 (2010).
- [18] K. Baumann, R. Mottl, F. Brennecke, and T. Esslinger, Exploring Symmetry Breaking at the Dicke Quantum Phase Transition, *Phys. Rev. Lett.* **107**, 140402 (2011).
- [19] K. J. Arnold, M. P. Baden, and M. D. Barrett, Self-Organization Threshold Scaling for Thermal Atoms Coupled to a Cavity, *Phys. Rev. Lett.* **109**, 153002 (2012).
- [20] F. Piazza, P. Strack, and W. Zwerger, Bose-Einstein condensation versus Dicke-Hepp-Lieb transition in an optical cavity, *Annals of Physics* **339**, 135 (2013).
- [21] J. Klinder, H. Keßler, M. Wolke, L. Mathey, and A. Hemmerich, Dynamical phase transition in the open Dicke model, *Proc. Nat. Aca. Sci.* **112**, 3290 (2015).
- [22] Z. Zhiqiang, C. H. Lee, R. Kumar, K. J. Arnold, S. J. Masson, A. S. Parkins, and M. D. Barrett, Nonequilibrium phase transition in a spin-1 Dicke model, *Optica* **4**, 424 (2017).
- [23] M. Landini, N. Dogra, K. Kroeger, L. Hruby, T. Donner, and T. Esslinger, Formation of a Spin Texture in a Quantum Gas Coupled to a Cavity, *Phys. Rev. Lett.* **120**, 223602 (2018).
- [24] R. M. Kroeze, Y. Guo, V. D. Vaidya, J. Keeling, and B. L. Lev, Spinor Self-Ordering of a Quantum Gas in a Cavity, *Phys. Rev. Lett.* **121**, 163601 (2018).
- [25] Z. Zhang, C. H. Lee, R. Kumar, K. J. Arnold, S. J. Masson, A. L. Grimsmo, A. S. Parkins, and M. D. Barrett, Dicke-model simulation via cavity-assisted Raman transitions, *Phys. Rev. A* **97**, 043858 (2018).
- [26] A. Morales, D. Dreon, X. Li, A. Baumgärtner, P. Zupancic, T. Donner, and T. Esslinger, Two-mode Dicke model from nondegenerate polarization modes, *Phys. Rev. A* **100**, 013816 (2019).
- [27] X. Li, D. Dreon, P. Zupancic, A. Baumgärtner, A. Morales, W. Zheng, N. R. Cooper, T. Donner, and T. Esslinger, First order phase transition between two centro-symmetric superradiant crystals, *Phys. Rev. Res.* **3**, L012024 (2021).
- [28] S. Sachdev, *Quantum Phase Transitions*, 2nd ed. (Cambridge University Press, 2011).
- [29] E. Fradkin, S. A. Kivelson, and J. M. Tranquada, Colloquium: Theory of intertwined orders in high temperature superconductors, *Rev. Mod. Phys.* **87**, 457 (2015).
- [30] A. Morales, P. Zupancic, J. Léonard, T. Esslinger, and T. Donner, Coupling two order parameters in a quantum gas, *Nature Materials* **17**, 686 (2018).
- [31] J. Léonard, A. Morales, P. Zupancic, T. Esslinger, and T. Donner, Supersolid formation in a quantum gas breaking a continuous translational symmetry, *Nature* **543**, 87 (2017).
- [32] J. Lang, F. Piazza, and W. Zwerger, Collective excitations and supersolid behavior of bosonic atoms inside two crossed optical cavities, *New Journal of Physics* **19**, 123027 (2017).
- [33] Z. Wu, Y. Chen, and H. Zhai, Emergent symmetry at superradiance transition of a Bose condensate in two crossed beam cavities, *Science Bulletin* **63**, 542 (2018).
- [34] R. R. Soldati, M. T. Mitchison, and G. T. Landi, Multipartite quantum correlations in a two-mode Dicke model, *Phys. Rev. A* **104**, 052423 (2021).
- [35] J. Léonard, A. Morales, P. Zupancic, T. Donner, and T. Esslinger, Monitoring and manipulating Higgs and Goldstone modes in a supersolid quantum gas,

- [Science](#) **358**, 1415 (2017).
- [36] J. Keeling, M. J. Bhaseen, and B. D. Simons, Collective Dynamics of Bose-Einstein Condensates in Optical Cavities, [Phys. Rev. Lett.](#) **105**, 043001 (2010).
- [37] N. Liu, J. Lian, J. Ma, L. Xiao, G. Chen, J. Q. Liang, and S. Jia, Light-shift-induced quantum phase transitions of a Bose-Einstein condensate in an optical cavity, [Phys. Rev. A](#) **83**, 033601 (2011).
- [38] M. J. Bhaseen, J. Mayoh, B. D. Simons, and J. Keeling, Dynamics of nonequilibrium Dicke models, [Phys. Rev. A](#) **85**, 013817 (2012).
- [39] F. Mivehvar, H. Ritsch, and F. Piazza, Superradiant Topological Peierls Insulator inside an Optical Cavity, [Phys. Rev. Lett.](#) **118**, 073602 (2017).
- [40] P. Zupancic, D. Dreon, X. Li, A. Baumgärtner, A. Morales, W. Zheng, N. R. Cooper, T. Esslinger, and T. Donner, *P*-Band Induced Self-Organization and Dynamics with Repulsively Driven Ultracold Atoms in an Optical Cavity, [Phys. Rev. Lett.](#) **123**, 233601 (2019).
- [41] Y. Chen, Z. Yu, and H. Zhai, Superradiance of Degenerate Fermi Gases in a Cavity, [Phys. Rev. Lett.](#) **112**, 143004 (2014).
- [42] J. Léonard, *A Supersolid of Matter and Light*, [Doctoral thesis](#), ETH Zurich, Zurich (2017).